Journal of Medicinal Chemistry

pubs.acs.org/jmc

Article

Structure-Based Stabilization of Non-native Protein–Protein Interactions of Coronavirus Nucleocapsid Proteins in Antiviral Drug Design

Shan-Meng Lin,[○] Shih-Chao Lin,[○] Jia-Ning Hsu,[○] Chung-ke Chang,[○] Ching-Ming Chien, Yong-Sheng Wang, Hung-Yi Wu, U-Ser Jeng, Kylene Kehn-Hall, and Ming-Hon Hou*

Cite This: *J. Med. Chem.* 2020, 63, 3131–3141

Read Online

ACCESS | Metrics & More | Article Recommendations | Supporting Information

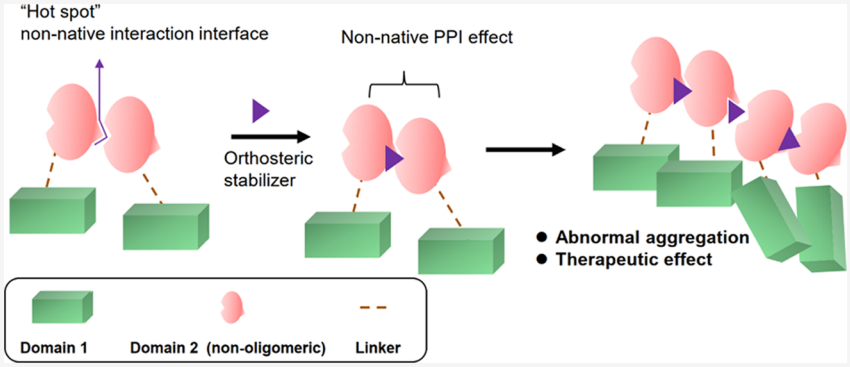

ABSTRACT: Structure-based stabilization of protein–protein interactions (PPIs) is a promising strategy for drug discovery. However, this approach has mainly focused on the stabilization of native PPIs, and non-native PPIs have received little consideration. Here, we identified a non-native interaction interface on the three-dimensional dimeric structure of the N-terminal domain of the MERS-CoV nucleocapsid protein (MERS-CoV N-NTD). The interface formed a conserved hydrophobic cavity suitable for targeted drug screening. By considering the hydrophobic complementarity during the virtual screening step, we identified 5-benzyloxygramine as a new N protein PPI orthosteric stabilizer that exhibits both antiviral and N-NTD protein-stabilizing activities. X-ray crystallography and small-angle X-ray scattering showed that 5-benzyloxygramine stabilizes the N-NTD dimers through simultaneous hydrophobic interactions with both partners, resulting in abnormal N protein oligomerization that was further confirmed in the cell. This unique approach based on the identification and stabilization of non-native PPIs of N protein could be applied toward drug discovery against CoV diseases.

INTRODUCTION

Small-molecule stabilization of protein–protein interactions (PPIs) is an extremely promising strategy in drug discovery. It can be used to treat cancers and viral infections.[1−3] Stabilizing PPIs with small molecules may be allosteric or direct (also called orthosteric). This process alters the oligomerization equilibrium of the protein and enables small molecules to modulate its physiological function.[4−7] The anticancer drug paclitaxel, for example, allosterically enhances microtubule structure assembly by binding to β-tubulin.[8,9] On the other hand, rapamycin, another anticancer agent, binds directly to the interface between FKBP12 and mTOR and stabilizes the structure of the complex.[10] The most well-characterized PPIs suitable as targets for drug development form natively under physiological conditions. However, non-native interactions, which may form under extreme circumstances such as inside a crystal lattice, are also potential drug targets. For example, nucleozin exerts its antiviral activity by stabilizing the non-native PPI interface between the two neighboring nucleoprotein trimers within the influenza virus, which results in abnormal protein oligomerization and loss of viral viability.[11]

Middle East respiratory syndrome coronavirus (MERS-CoV) belongs to the betacoronavirus (β-CoVs) family. It causes severe respiratory distress with a high mortality rate in humans.[12−14] Recently, a closely related novel coronavirus, coronavirus disease 2019 (COVID-19), caused an outbreak of pneumonia in Wuhan, which further underscored the risk of CoVs to the global public health.[15,16] However, there is no

Received: November 19, 2019
Published: February 27, 2020

https://dx.doi.org/10.1021/acs.jmedchem.9b01913
J. Med. Chem. 2020, 63, 3131–3141

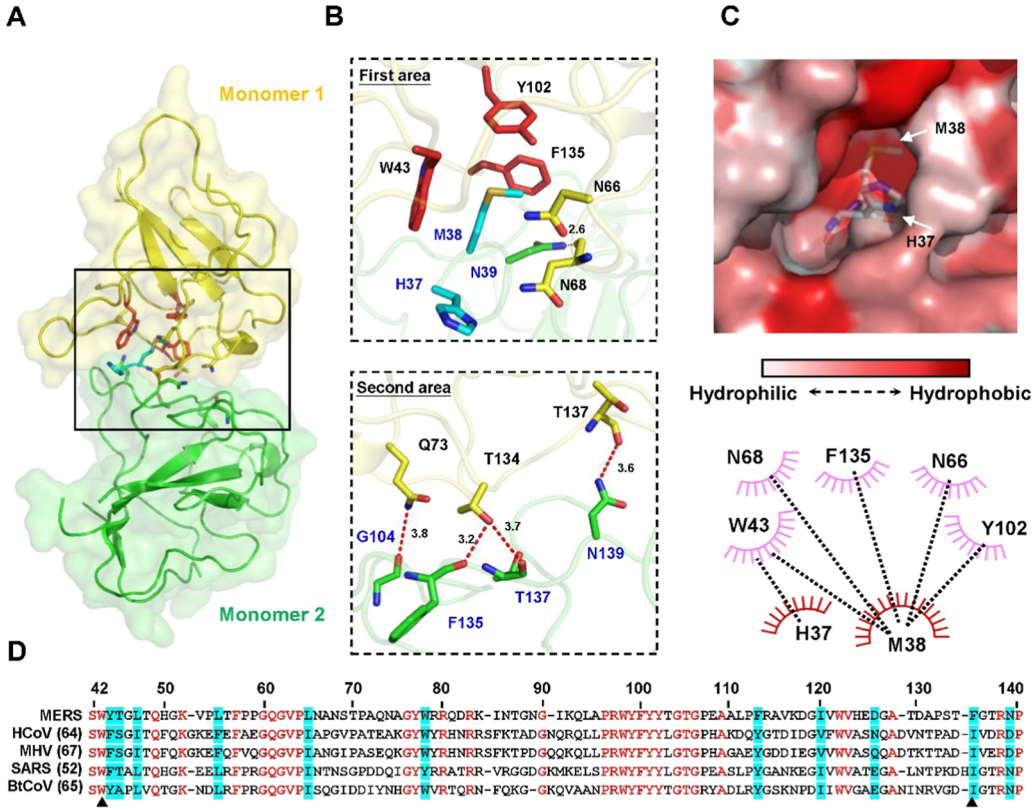

Figure 1. Structure and sequence of MERS-CoV N-NTD. (A) Overall structure of the MERS-CoV N-NTD dimer containing monomers 1 and 2 is depicted as a cartoon and colored yellow and green, respectively. Residues involved in dimerization are shown as sticks and highlighted in (B). (B) Interactions among MERS-CoV N-NTDs. Dimerization is mediated mainly by vector-fusion residues interacting with the conserved hydrophobic regions on the core structure (first area) along with the residues surrounding it (second area). Interacting residues on monomers 1 and 2 are labeled in black and blue, respectively. Vector-fusion and conserved hydrophobic regions are colored cyan and red, respectively. The color of all other interacting residues is the same as that for each monomer in (A). Polar contacts are indicated with red dashed lines. (C) Upper panel: close-up of the interacting region of vector-fusion residues. The surface was colored according to the hydrophobicity level at the protein surface. Vector-fusion residues (black) are shown as sticks to emphasize the hydrophobic pocket. Lower panel: 2D diagrams of the interaction between the hydrophobic pocket and the vector-fusion residues. The latter are labeled in black. The hydrophobic contacts are indicated with black dashed lines. (D) Sequence alignment of various CoV N proteins in the N-terminal region. Red letters indicate strictly conserved residues. Cyan indicates conservative substitution sites. Hydrophobic regions involved in unusual dimerization are indicated by black triangles.

effective treatment for CoVs. Thus, there is an urgent need to develop new antiviral agents against CoVs.[14,17] MERS-CoV packages its genome in a nucleocapsid (N) protein and forms a ribonucleoprotein (RNP) complex. The RNP is essential for viral transcription and assembly. Several studies suggested that the modulation of CoV N protein oligomerization by small molecules is a feasible antiviral drug development strategy.[18,19] The CoV N protein is organized into the N-terminal domain (NTD) and the C-terminal domain (CTD), with both domains participating in RNA binding.[20,21] All CoV N-NTD structures are folded in a monomeric conformation. In contrast, the CoV N-CTDs are always dimeric and are responsible for N protein oligomerization via protein−protein interactions.[22,23]

Here, we report the crystal structure of MERS-CoV N-NTD in a non-native dimeric configuration. We used the non-native dimer interface as the target in virtual screening for an orthosteric stabilizer. To this end, we considered the binding scores and hydrophobic complementarity of the acquired poses, and further selected the potential leads P1−P3 from Acros and ZINC drug databases. Of these, only 5-benzyloxygramine (P3) had both antiviral and stabilizing activities on the N protein. Small-angle X-ray scattering (SAXS) and cell-based assays showed that P3 induces abnormal full-length N protein oligomerization in vitro and at the cell level. We also described the structure of MERS-CoV N-NTD complexed with 5-benzyloxygramine and revealed its stabilizing mechanism. Our findings provide insight into the development of a new therapeutic approach based on stabilizing a non-native protein interaction interface. It may lead to the discovery and development of new treatments for various infectious diseases.

RESULTS

Structure of the N-Terminal Domain of the MERS-CoV N Protein. We determined the crystal structure of MERS-CoV N-NTD by molecular replacement (MR) using the structure of HCoV-OC43 N-NTD (PDB ID: 4J3K) as the search model.[24] The final structure was refined to R-factor and R-free values of 0.26 and 0.29, respectively, at a resolution of 2.6 Å (Table S1). Each asymmetric unit contained four N-NTD molecules assembled into two identical dimers with an overall RMSD of 0.28 Å between the dimers (Figure S1A,B). The monomers shared a similar structural core preceded by a flexible region (Figure S1D). The core consisted of a five-stranded antiparallel β-sheet sandwiched between loops arranged in a right-handed, fist-shaped structure conserved

https://dx.doi.org/10.1021/acs.jmedchem.9b01913
J. Med. Chem. 2020, 63, 3131−3141

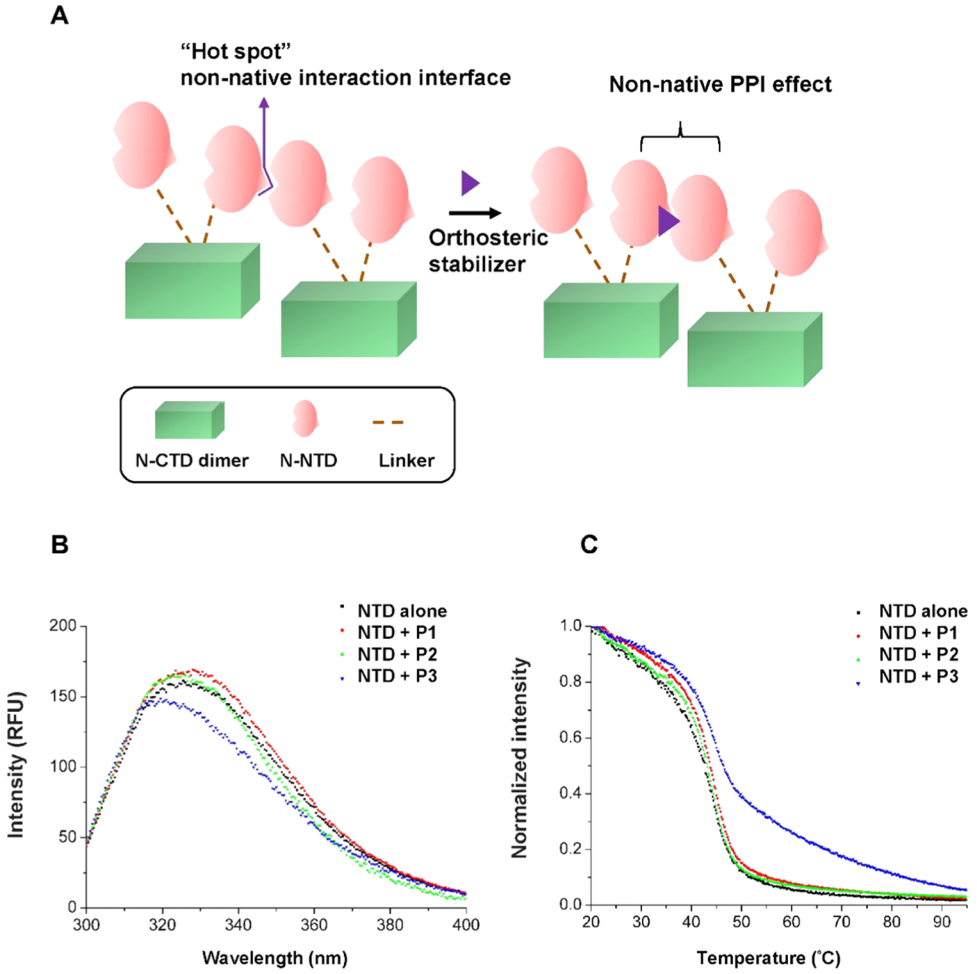

Figure 2. Compound P3 was a potent stabilizer of the MERS-CoV N protein. (A) Schematic depicting the rationale used in designing the allosteric stabilizer of this study. An orthosteric stabilizer may be used to bind to the non-native interaction interface of the N protein and stabilize the abnormal interaction between proteins. (B) Conformation and (C) stability analyses were performed based on the FL spectra of NTD (1 μM) incubated with P1−P3 (10 μM) for 1 h with a buffer consisting of 50 mM Tris-HCl (pH 8.3) and 150 mM NaCl.

among the CoVs.[25] In our structure, however, the loop connecting strands β2 and β3 protruding out of the core into other CoV N proteins was absent. Unlike the reported structures that have a monomeric conformation, our structure was atypically dimeric.

Figure 1B shows the details of the interactions in the MERS-CoV N protein dimer. We named the units monomer 1 and monomer 2 (Figure 1A). According to the amino acid composition of the binding site on monomer 2, we divided the dimeric interface into two areas: one located on the N-terminus flexible region and the other on the loop between β4 and β5 of the N protein. In the first area, W43, N66, N68, Y102, and F135 of monomer 1 generated a conserved hydrophobic pocket permitting the side chain of M38 of monomer 2 to enter this hole by a hydrophobic contact (Figure 1C,D). H37 and N39 of monomer 2 were packed against W43 and F135 of monomer 1, respectively, and contributed to the hydrophobic interaction. The side chains of N39 of monomer 2 formed one hydrogen bond with the N68 backbone in monomer 1 at a distance of 2.6 Å. The second area was relatively more hydrophilic. The main chain oxygens of G104, F135, and T137 of monomer 2 formed three hydrogen bonds with the side chains of Q73 and T134 of monomer 1 at distances of 3.8, 3.2, and 3.7 Å, respectively. The side chain of N139 on monomer 2 formed a hydrogen bond with the main chain oxygen of T137 on monomer 1 at a distance of 3.6 Å. The interactions of the first and second areas comprise buried surface areas (BSA) of 289 and 103 Å^2, respectively. The small surface area buried at the interface accounts for ~5 kcal mol^{-1} binding energy,[26] which translates to a dissociation constant of ~200 mM. Thus, the dimer described here is unique in that it is non-native and relies on vector-fusion residues (H37 and M38) to maintain its dimeric status. This property may also explain why the present structure has an oligomeric status different from previously reported structures for the CoV N protein.[24,27−30] We used cross-linking experiments to analyze the oligomeric capacity of MERS N-NTD containing the vector-fusion residues in solution. MERS N-NTD had a dimeric conformation in solution. Our structure indicated that W43 played an essential role in forming the hydrophobic pocket accommodating the vector-fusion residues and, therefore, mediated the N-NTD dimer formation. The W43A mutation significantly reduced the oligomeric tendency of N-NTD (Figure S1C). This further supports that the "exogenous residues" encoded by the vector backbone mediated the formation of the non-native dimer. We also superimposed the previously published structure of MERS-CoV N-NTD (PDB ID: 4ud1)[27] containing a native

https://dx.doi.org/10.1021/acs.jmedchem.9b01913
J. Med. Chem. 2020, 63, 3131−3141

N-terminal flexible region with our dimer structure. The side chain of N38 in the native structure could not interact with the hydrophobic pocket as the former is hydrophilic and short (Figure S1E). Thus, it may be possible to utilize small compounds to replace the vector-fusion residues and stabilize the PPI through hydrophobic interactions.

Direct Targeting of the Non-native Dimer Interface for Antiviral Screening. We performed a structure-based virtual screening by targeting W43 in the hydrophobic pocket of the N-NTD dimeric interface. H37 and M38 were removed from the template to identify compounds that could replace the vector-fusion residues and, therefore, contribute to the stabilizing effect (Figures 2A and S2A,B). We chose the highest-scoring hits, listed in Table S2, based on shape complementarity, the presence of aromatic moieties, and the ability to stack onto W43 of N-NTD. Because the formation of the non-native dimers was primarily mediated by hydrophobic interactions in our structure (Figure 1C,D), we next considered the hydrophobic complementarity between the acquired ligands and N-NTD in the form of the lipophilic match surface ($S_{L/L}$).[31] We also took into account the ability of the drug to permeate cells by aiming for lower topological polar surface areas (TPSA). Based on the above criteria, three compounds were finally chosen for further study. Benzyl-2-(hydroxymethyl)-1-indolinecarboxylate (P1) and 5-benzyloxygramine (P3) had higher $S_{L/L}$ and docking scores and lower TPSA. The clinical drug etodolac (P2) had a comparable $S_{L/L}$ but a lower docking score. It too was selected as a candidate. However, only P3 induced a comparatively larger blue shift in the intrinsic N-NTD fluorescence spectrum, indicating that the microenvironment surrounding the tryptophans of the protein increased in rigidity and hydrophobicity in the presence of P3.[32] The result also indicated that P3 bound more tightly to the N protein than P1 or P2 by interacting with the W43 pocket (Figure 2B). Fluorescent thermal stability assays disclosed that the N-NTD denaturation melting temperature had increased from 42 to 45 °C when P3 was added. The sigmoidal melting curve for MERS-CoV N-NTD changed in the presence of P3. The delay in protein denaturation suggests that P3 stabilized the MERS-CoV N-NTD dimer structure (Figure 2C). We then measured the cytotoxic concentration (CC_{50}) and effective concentration (EC_{50}) for each compound using Vero E6 cells infected with MERS-CoV. Table 1 shows that P3 had a favorable therapeutic index among the lead compounds tested in this study. Therefore, P3 is an excellent candidate inhibitor against MERS-CoV.

Structural Model of P3-Induced MERS-CoV N Protein Aggregation. We used SAXS to assess the effects of P3 on the full-length MERS-CoV N protein structure. The fitted distance distribution function of the protein with and without P3 are shown in Figure 3A. P3 increased the maximum dimension (D_{max}) and radius of gyration (R_g) of the protein from 207 to 230 Å and from 58 to 65 Å, respectively. Thus, the size of the MERS-CoV N protein in solution was altered upon binding to P3.

The presence of multiple intrinsically disordered regions in the N protein precluded the determination of its structure by X-ray crystallography. Instead, we used rigid body modeling of the SAXS data with the N-terminal domain (NTD; solved in this study) and the C-terminal domains (CTD, PDB ID: 6G13).[23] In this way, we obtained structural models for the free N protein and its complex with P3 (Figure 3B,C). Excellent fits were obtained. Representative structural models for the full-length protein without and with P3 are shown in Figure 3D,E, respectively. The free N protein formed a tetramer through CTD with the NTD freely hanging in solution (Figure 3D). The conformation of the solution was consistent with structures previously reported for other CoV N proteins.[33] The N-P3 complex formed a compact hexadecamer with a sunburst configuration (Figure 3E). The CTDs formed a central ring and non-native NTD dimers formed "spikes" protruding from the ring. Consistent with ligand-induced aggregation, we observed a "blue shift" in the fluorescence spectrum of the full-length MERS-CoV N protein in the presence of P3 (Figure 3F). The addition of P3 also delayed N protein thermal denaturation and changed the shape of the denaturation curve, further suggesting that large protein aggregates formed in the presence of P3 (Figure 3G). The structure explains how N-NTD dimerization decreased MERS-CoV viability. The N protein packages the viral genome into an RNP complex. Several models for N-CTD dimer assembly have been proposed for the formation of filamentous RNPs.[33] All of the proposed interfaces between N-CTD dimers occurred on the side-faces of the CTD cuboid perpendicular to the proposed RNA-binding surface (Figure 3H). Combinatorial use of any region on the side-faces of the CTD dimer cuboid may facilitate manipulation of the RNP length and curvature without obstructing the RNA-binding surface.[28,34] However, the SAXS results indicated that N-CTD aggregation occurred on the β-sheet floor of the CTD cuboid. For this reason, the RNA-binding surface of the CTD is occluded by the neighboring CTD on the ring and by the non-native NTD dimer making direct contact with the CTD (Figures 3H and S3). In addition, the CTD cuboids in the aggregation naturally form a topologically closed octamer, leaving no open ends for further addition of CTD cuboids to form a long filamentous RNP. Both the loss of the RNA-binding surface and the inability to incorporate further N protein molecules beyond an octamer may inhibit the formation of the RNP. Therefore, P3 may inhibit MERS-CoV RNP formation by inducing N protein aggregation.

P3 Inhibits MERS-CoV by Inducing N Protein Aggregation. We demonstrated that P3 had the best characteristics as a therapeutic candidate. To determine the anti-MERS-CoV activity of P3 in the cell, the effects of P3 incubation on extracellular viral titers and intracellular viral RNA levels were assessed by plaque assays on Vero E6 cells (Figure 4A) and by RT-qPCR (Figure 4B), respectively. At 50 μM, P3 marginally affected the viral titer after 48 h but suppressed viral RNA replication by 40%. At 100 μM, P3 halted both viral production and replication after 48 h. This result proved the capacity of P3 as an antiviral compound. We then examined MERS-CoV N protein distribution and expression in the infected cells with or without P3 treatment

Table 1. CC_{50} and EC_{50} and Therapeutic Indexes of Lead Compounds

quantal dose−response relationship (μM)			
compound	CC_{50}[a]	EC_{50}[b]	TI[c] (CC_{50}/EC_{50})
P1	459.69	>100	NA[d]
P2	569.77	>100	NA[d]
P3	805.32	32.1	25.1

[a]CC_{50}: Half maximal toxicity concentration. [b]EC_{50}: Half maximum effective concentration. [c]TI: Therapeutic index. [d]NA: Nonavailable.

https://dx.doi.org/10.1021/acs.jmedchem.9b01913
J. Med. Chem. 2020, 63, 3131−3141

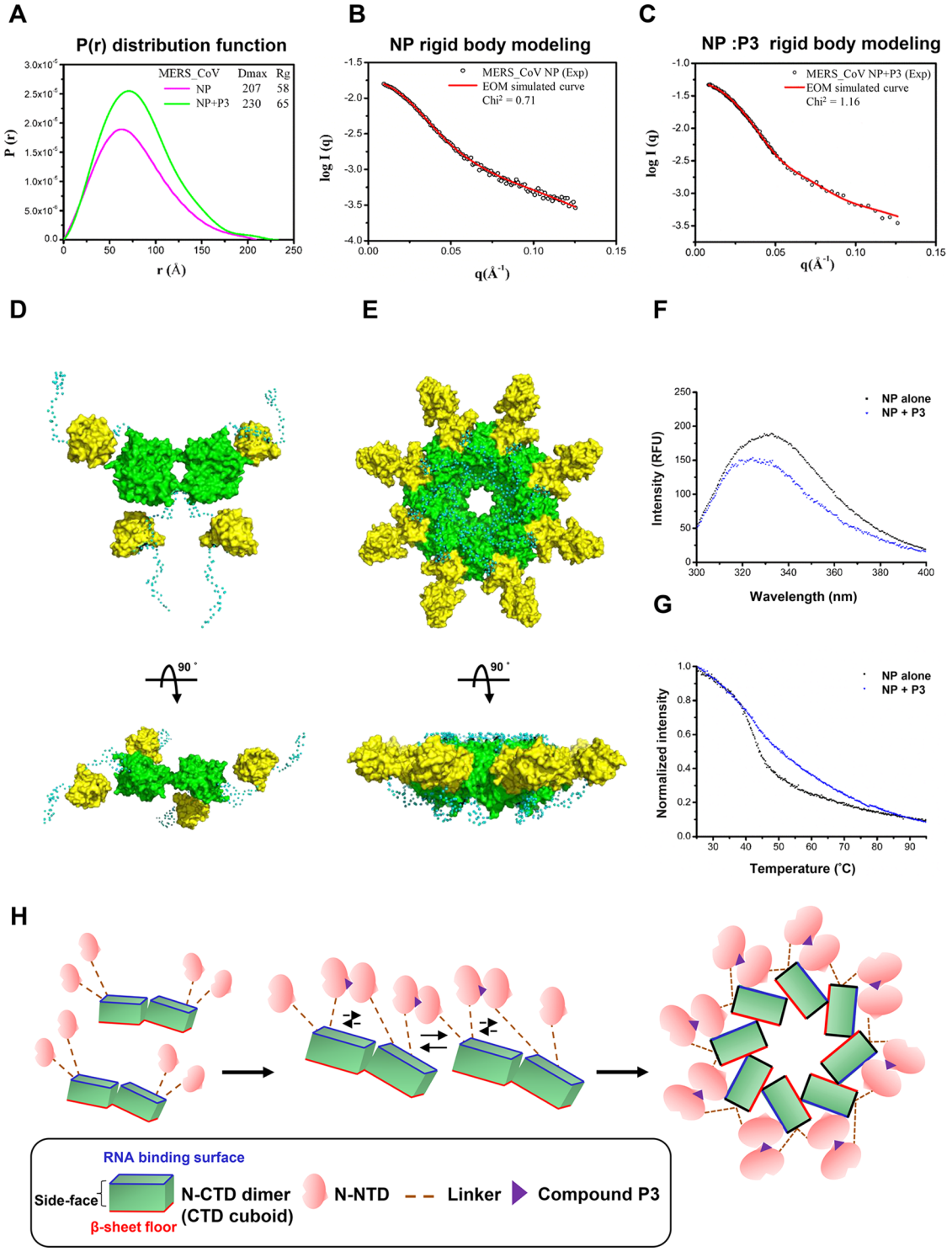

Figure 3. P3-induced abnormal aggregation on the full-length MERS-CoV N protein. (A–E) SAXS analysis of the full-length MERS-CoV N protein. (A) Normalized results from GNOM showing pairwise distance distribution $P(r)$ and maximum distance. The radius of gyration fitted to 207 and 230 Å for the N protein and the N-P3 complex, respectively. "r" represents pairwise distances. (B, C) Scattering profiles of the N protein (B) and the N-P3 complex (C) and normalization fitting with GNOM (dashed lines). (D, E) Representative models of the N protein (D) and the N-P3 complex (E) generated by CRYSOL simulations of the SAXS data. Only α carbons are shown. NTD (yellow), CTD (green), and disorder region (cyan). (F, G) Conformation (F) and stability (G) analyses based on FL spectra of the MERS-CoV N protein (1 μM) incubated with P3 (10 μM) for 1 h in a buffer consisting of 50 mM Tris-HCl, 150 mM NaCl (pH 8.3). (H) Schematic of the P3 inhibition mechanism. Left panel: in the absence of RNA, N proteins organize as a dimeric building block contributed by N-CTD dimerization. Middle panel: P3 promoted the dimerization of N-NTDs from different building blocks, by which the distance between CTD cuboids was shortened and N protein aggregation occurred. Right panel: octameric conformation of building blocks buried in the RNA-binding surface of N-CTDs. It hindered the formation of filamentous ribonucleocapsids.

https://dx.doi.org/10.1021/acs.jmedchem.9b01913
J. Med. Chem. 2020, 63, 3131−3141

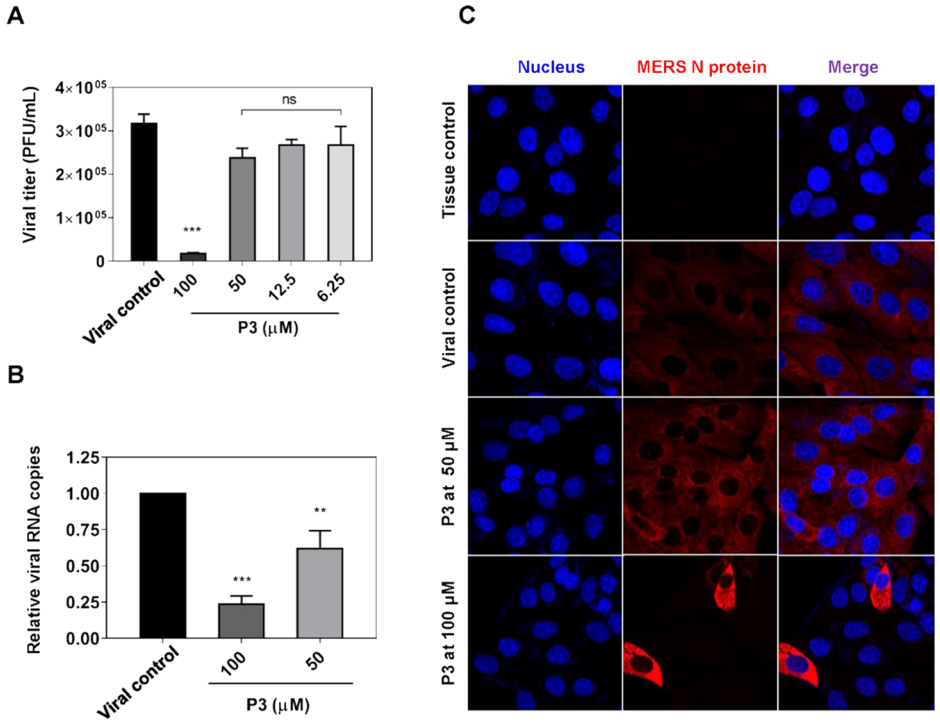

Figure 4. Compound P3 was a potential inhibitor against MERS-CoV. (A, B) Viral titers (A) and RNA (B) of MERS-CoV measured by plaque assay and RT-qPCR, respectively, decreased after P3 treatment for 48 h. Relative RNA levels were determined by comparing MERS alone at each time point. GAPDH RNA was the internal control. All values are presented as mean ± SE (standard error of mean). One-way Anova was used for statistics (*p < 0.05, **p < 0.01, ***p < 0.001). (C) MERS-CoV nucleocapsid protein decreased after 48 h P3 treatment. Nucleocapsid protein expressions (red) were examined under a confocal microscope at ×680. Nuclei were stained blue with DAPI.

to confirm our SAXS findings. Immunofluorescence microscopy (Figure 4C) showed condensation of the intracellular N protein fluorescence signal in infected Vero E6 cells treated with 50 μM P3. Thus, P3 may induce intracellular N protein aggregation. At 100 μM, P3 suppressed N protein expression in most cells. However, a few presented with intense N protein signals. P3 may have restrained the MERS-CoV N proteins inside the infected cells that promoted the formation of new virions that could not be released. In this way, the adjacent cells could not be infected with MERS-CoV. The data, therefore, suggest that P3 may inhibit MERS-CoV by inducing abnormal aggregation of the N protein inside the cell. This finding is consistent with the results of our structure-based assays.

Crystal Structure of MERS-CoV N-NTD Complexed with Potent Compounds. We attempted to obtain crystals of MERS-CoV N-NTD in complex with compounds P1, P2, and P3 by cocrystallization or ligand-soaking. With the exception of P2, the complex structures of N-NTD with P1 and P3 were solved at resolutions of 3.09 and 2.77 Å, respectively (Table S1). The overall structures of the complexes resembled that of apo-MERS-CoV. Both complexes revealed well-defined unbiased densities in the dimer interface and permitted detailed analysis of the interactions between the compounds and MERS-CoV N-NTD (Figure 5). The interactions between the N protein and each compound were calculated with the Discovery Studio Client (v19.1.0.18287). Most interactions were hydrophobic contacts, which were consistent with our selection rationale. In the P1 complex, N68, F135, and D143 on monomer 1 and V41, G106, P107, and T137 on monomer 2 packed against P1 to create a dimer (Figure 5A). In addition, two nonbonding interactions were detected between P1 and the monomers. There was a π-anion interaction between the benzene ring of the P1 indoline moiety and D143 of monomer 1. There was also a π-donor hydrogen bond between the other P1 benzene ring and the T137 side chain of monomer 2 (Figure 5B). Relative to P1, P3 bound more deeply into the dimer interface and interacted with a larger number of residues on both N-NTD monomers. The amino acid composition of this binding region was W43, N66, N68, S69, T70, N73, and F135 on monomer 1 and V41, G104, T105, G106, A109, and T137 on monomer 2. These residues along with P3 generated a massive hydrophobic driving force allowing the proteins and ligands to pack against each other and stabilize the dimeric conformation of the N protein (Figure 5C). Several nonbonding interactions were also observed at the P3-binding site. These included the interaction between the P3 benzene ring and N68 of monomer 1 and A109 of monomer 2 via π-lone pair and π-alkyl interactions. The dimethylaminomethyl moiety of P3 was a major source of nonbonding interactions. Three π-cation interactions formed between this moiety and the aromatic groups of W43 and F135 in monomer 1. This moiety also formed a π-lone pair interaction with N66 and a π-sigma interaction with W43 of monomer 1 (Figure 5D). The structural analyses explain the comparatively stronger binding of P3 to N-NTD (Figure 2B) and corroborated the thermal stabilization effects (Figure 2C) and antiviral activities (Table 1) of the compounds.

DISCUSSION AND CONCLUSIONS

The use of small molecules to stabilize PPI interfaces has been shown to be a viable approach for the development of new therapeutics. Most compounds created by structure-based

https://dx.doi.org/10.1021/acs.jmedchem.9b01913
J. Med. Chem. 2020, 63, 3131−3141

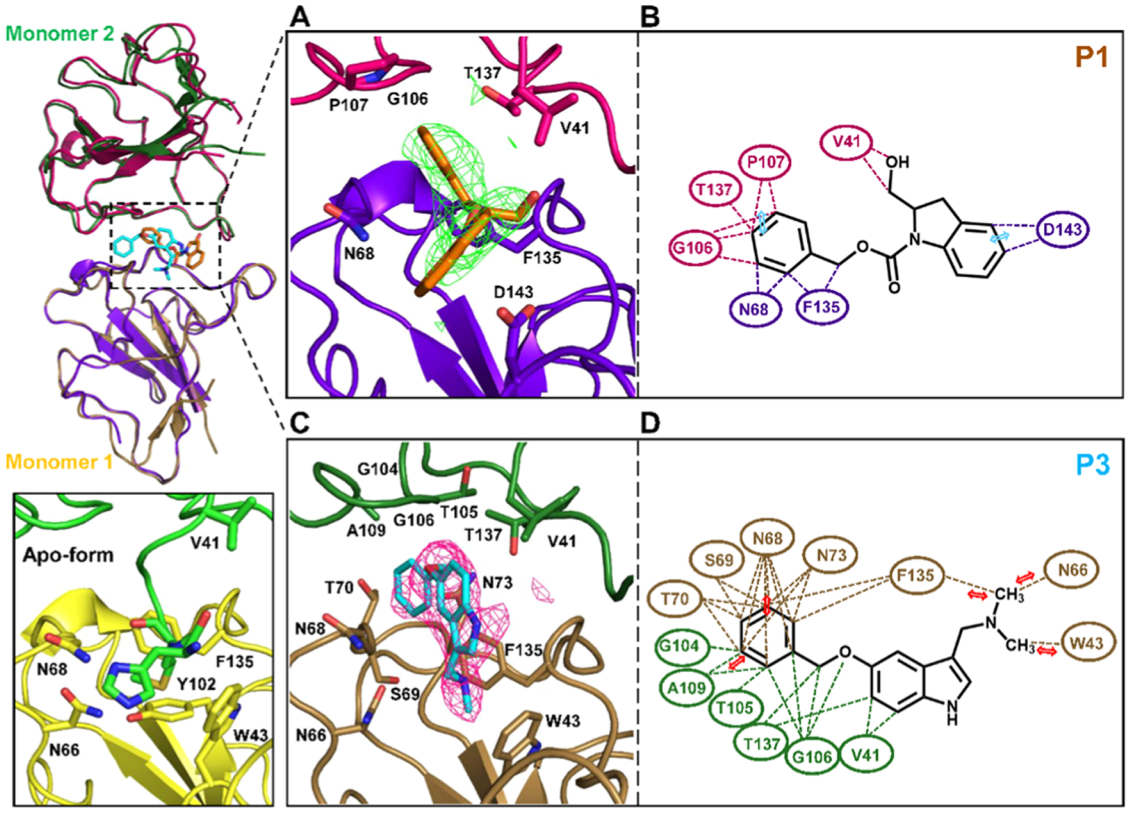

Figure 5. Structures of MERS-CoV N-NTD complexed with potent compounds. The structures were solved using HCoV-OC43 N-NTD (PDB:4J3K) as the search model.[24] Left panel: (Upper) structural superimposition of the MERS-CoV N-NTD:P1 complex (monomers 1 and 2 are in purple and pink, respectively) and the MERS-CoV N-NTD:P3 complex (monomers 1 and 2 are in brown and green, respectively) with compounds depicted as stick structures. (Lower) Interactions involving vector-fusion residues in the non-native dimer of the apoprotein shown for comparison with (A) and (B). Color is the same as in Figure 1A. Right panel: detailed interactions among MERS-CoV N-NTD and P1 (A, B) and P3 (C, D). Different Fo−Fc maps were contoured at ∼2.5 σ. (A) Detailed stereoview of interactions at the P1-binding site. The color of each monomer is the same as in the left panel. Residues constructing the P1-binding pocket are labeled and showed as sticks. (B) Schematic of P1 bound to MERS-CoV N-NTD. Hydrophobic contacts between P1 and each monomer are displayed as dashed lines. Nonbonding interactions are indicated by cyan arrows. (C) Detailed stereoview of interactions at the P3-binding site. The color of each monomer is the same as in the left panel. Residues belonging to the P3-binding pocket are labeled and shown as sticks. (D) Schematic of P3 bound to MERS-CoV N-NTD. Hydrophobic contacts between P3 and each monomer are displayed as dashed lines. Nonbonding interactions are indicated by red arrows.

design to manipulate the PPI depend on detailed knowledge of the native interacting interfaces.[35−37] In contrast, most of the compounds with therapeutic potential that stabilize non-native PPI interfaces were discovered by chance alone.[38] The anti-influenza compound nucleozin was initially discovered using a chemical genetics approach, and its ability to stabilize non-native nucleoprotein oligomers was elucidated much later.[39,40] Swinholide A, a cytotoxic marine macrolide, has been known to disrupt the actin cytoskeleton and act as an anticancer agent, but it took ten years to discover that it stabilized G-actin as a non-native homodimer complex.[41−43] However, these examples did underscore the importance of hydrophobicity as a crucial factor stabilizing protein−protein and protein−ligand associations.[44] Here, we demonstrated the possibility of using the hydrophobic interactions on non-native interfaces as targets for virtual screening. Combined with suitable selection criteria focusing on both shape and hydrophobic complementarities between the ligand and the receptor, small-molecule compounds that stabilize non-native PPIs may be identified in a rational manner. Using the above approach, we successfully identified a compound P3 that affected the biochemical activity of our target protein and showed efficacy against our target pathogen MERS-CoV (Figures 2 and 4). P3-mediated non-native MERS-CoV N-NTD dimerization induced abnormal N protein aggregation by influencing the oligomeric behavior of N-CTD and eventually halting its function in RNP formation. To the best of our knowledge, this structure-based strategy for targeting non-native interfaces has never been proposed for therapeutic design. Thus, non-native interaction interfaces in proteins may comprise a new drug development target class. For β-coronaviruses such as MERS-CoV, the amino acids comprising the non-native interaction interface on N-NTD are relatively conserved. The hydrophobic pocket surrounding W43 and F135 on monomer 1 is shared among other β-coronaviruses.[24,28] The interacting surface on monomer 2, which includes G104, T105, G106, and A109, is also highly conserved (Figure S4). This conservation may provide certain advantages when developing compounds with broad-spectrum activity against a target pathogen family, including COVID-19. When we tested P3 on mouse hepatitis virus (MHV), we observed a reduction in viral titer, indicating that P3 may also inhibit MHV replication (Figure S5). On the other hand, targeting non-native interaction interfaces is not trivial. As interface formation is induced by an external agent, computations aimed at predicting native PPI structures may not be able to identify potential non-native interfaces. Nevertheless, several stratagems may assist in the identification of potential non-native interaction interfaces. One strategy is to

https://dx.doi.org/10.1021/acs.jmedchem.9b01913
J. Med. Chem. 2020, 63, 3131−3141

search for target protein structures with crystal packing contacts known to be biologically irrelevant. Another approach is to identify weakly interacting sites through NMR chemical shift perturbation and hydrogen-deuterium exchange MS.[45] Once these potential non-native interaction interfaces are identified, standard screening and then functional characterization may be conducted for small compounds that bind to the interface.

To summarize, we demonstrated that non-native interaction interfaces might form when proteins abnormally oligomerize. Using the MERS-CoV N protein as an example, we showed that non-native interfaces might serve as targets for small-molecule, structure-based screening. We also proposed several stratagems to rationally identify potential non-native interface targets for screening. We believe that we have discovered and tested an alternative drug discovery paradigm that could help expand the repertoire of lead compounds against various pathogens.

EXPERIMENTAL SECTION

Chemicals. The compounds P1, P2, and P3 were purchased from Maybridge Chemical Company, TCI Chemicals, and Sigma-Aldrich Corporation, respectively. The reagents used in this study were purchased from Sigma Chemical Co. (St. Louis, MO). The purity of all compounds is higher than 95% and was used without further purification.

Cloning, Protein Expression, and Purification. The MERS-CoV N proteins were prepared according to previously described methods.[46] In brief, the cDNA fragments of MERS-CoV N proteins were cloned into a pET-28a expression vector (Merck, Darmstadt, Germany) containing a histidine tag-encoding sequence. Vectors encoding the single mutants N39A, N39G, and W43A were generated using the *QuikChange* site-directed mutagenesis protocol with the primers listed in Table S3. The vectors were transformed into *Escherichia coli* BL21 (DE3) pLysS cells. The cells were grown to an optical density range of 0.6−0.8 at 600 nm at 37 °C and protein expression induced with 1.0 mM isopropyl β-D-1-thiogalactopyranoside (IPTG), followed by incubation at 10 °C for 24 h. The cells were harvested by centrifugation (6000*g*, 12 min, 4 °C) and resuspended in lysis buffer (150 mM NaCl, 50 mM Tris-HCl, 15 mM imidazole, and 1 mM PMSF; pH 7.5). The cells were lysed by sonication and centrifuged (10000*g*, 40 min, 4 °C) to remove debris. The supernatant was purified by injection into a Ni−NTA column (Merck, Darmstadt, Germany) and eluted with buffer containing imidazole at a gradient range of 15−300 mM. Pure protein fractions were collected, dialyzed with low-salt buffer, concentrated, and quantified by the Bradford method (BioShop Canada Inc., Burlington, ON, Canada).

Crystallization and Data Collection. MERS-CoV N-NTD crystals were grown as previously described:[46] MERS-CoV N-NTD was crystallized at room temperature (~25 °C) by the sitting-drop vapor-diffusion method. A protein solution (2 μL; 10 mg mL^{-1}) was mixed with an equal volume of crystallization solution consisting of 75 mM ammonium sulfate, 2 mM NaBr, and 29% PEG 3350 (Sigma-Aldrich Corp., St. Louis, MO) and equilibrated against a 300 μL solution. MERS-CoV N-NTD:P3 co-crystals were obtained using a crystallization solution containing 2 mM P3. MERS-CoV N-NTD crystals in complex with P1 were obtained by soaking native MERS-CoV N-NTD crystals for 90 s at room temperature in a crystallization solution containing 2 mM P1. Diffraction datasets for MERS-CoV N-NTD alone and in complex with P1 were collected at beamline 13B1 of the Taiwan Light Source (TLS) of the National Synchrotron Research Center (NSRRC; Hsinchu City, Taiwan). Diffraction of the MERS-CoV N-NTD:P3 complex was performed at the beamline SP44XU of SPring-8 (Hyogo, Japan).

Structural Determination and Refinement. Diffraction data were processed and scaled with HKL-2000 software. The structures were solved by molecular replacement (MR) in Phenix[47] using HCoV-OC43 N-NTD (PDB:4J3K) as the search model.[24] The initial models were rebuilt and refined by Coot[48] and Phenix. Structures were visualized using PyMOL (The PyMOL Molecular Graphics System, version 2.3.0).[49]

Chemical Cross-Link Assay. Protein solutions containing 40 μM of wild-type or mutated MERS-CoV N-NTD were incubated with glutaraldehyde at a final concentration of 1% v/v. The reaction was conducted at room temperature for 10 min and quenched with the addition of 1 M Tris-HCl (pH 7.5). The samples were then stored on ice and analyzed by sodium dodecyl sulfate-polyacrylamide gel electrophoresis (SDS-PAGE).

Discovery of Orthosteric PPI Stabilizers for MERS N Protein. To screen for compounds that induce hydrophobic PPI between MERS N-NTDs, a model of dimeric MERS-CoV N-NTD without the H37 and M38 residues was used in virtual drug screening. The Sigma-Aldrich, Acros Organics, and ZINC drug databases were screened with LIBDOCK molecular docking software to obtain compounds acting on the N protein. The N protein binding pocket was represented by a set of spheres. Each compound in the database was docked in a pocket comprising W43. The hydrophobic complementarity between ligands and receptors was calculated with PLATINUM.[31] Compounds with higher docking scores are listed in Table S2.

Fluorescence Measurements. Fluorescence assays were performed in a buffer consisting of 50 mM Tris-HCl (pH 8.3) and 150 mM NaCl. One micromolar N protein was incubated either with the control buffer or each compound (10 μM) at 4 °C for 1 h. Tryptophan fluorescence was acquired with a Jasco FP-8300 fluorescence spectrometer (JASCO International Co. Ltd., Tokyo, Japan) at an excitation wavelength of 280 nm and an emission wavelength range of 300−400 nm.

Thermostability Measurements. Thermostability assays were conducted in a buffer consisting of 50 mM Tris-HCl (pH 7.5) and 150 mM NaCl and with a JASCO FP-8300 fluorescence spectrometer (JASCO International Co. Ltd., Tokyo, Japan). One micromolar N protein was incubated either with the control buffer or each compound (10 μM) at 4 °C for 2 h. UV absorbance vs temperature profiles were acquired by ramping the temperature from 4−95 °C at a 1 °C min^{-1} and recording the absorbance at 280 nm every 0.5 min.

Determining CC_{50} and EC_{50} of Hit Compounds. Vero E6 cells were infected with MERS-CoV with M.O.I = 0.1 and treated with lead compounds for 48 h. Cell viability was determined by the neutral red uptake assay. CC_{50} and EC_{50} were determined by % cell viability. CC_{50} was determined for cells treated with drugs only. EC_{50} was determined for MERS-infected cells after drug treatments.

Small-Angle X-ray Scattering (SAXS) Experiments. SAXS experiments were performed at the BL23A SAXS beamline at the TLS of NSRRC, using a monochromatic X-ray beam (λ = 0.828 Å), with an integrated HPLC system of an Agilent-Bio SEC-3 300 Å column (Agilent Technologies, Inc. Santa Clara, CA). Protein samples (44 μM MERS-CoV N and MERS-CoV N:P3 complex prepared by incubating the 44 μM native protein with 440 μM P3) were prepared in a buffer consisting of 50 mM Tris-HCl (pH 8.5) and 150 mM NaCl on ice for 1 h. Then, a 100 μL aliquot was injected into the column at a flow rate of 0.02 mL min^{-1}. After passing through the column, the sample solution was directed into a quartz capillary (2 mm dia.) for subsequent buffer and sample SAXS measurement at 288 K. The sample-to-detector distance of 2.5 m used covered a scattering vector q range of 0.01−0.20 $Å^{-1}$. Here, q is defined as $q = (4\pi/\lambda)\sin\theta$, with the scattering angle 2θ. Thirty-six frames were collected for each sample elution with an X-ray frame exposure time of 30 s. Frames of good data overlapping (namely, of low radiation damage effects) were merged for improved data statistics and analyzed to determine initial R_g using PRIMUS (version 3.1). The $P(r)$ distance distribution and D_{max} were calculated from the experimental scattering curve using GNOM (version 4.1). An ensemble optimization method (EOM) analysis was performed through the EMBL Hamburg web interface.[50] Modeling of the rigid body crystal structure was calculated and generated using CRYSOL (ATSAS Program Suite v. 2.8.2).[51] The

https://dx.doi.org/10.1021/acs.jmedchem.9b01913
J. Med. Chem. 2020, 63, 3131−3141

crystal structures of MERS-CoV NTD (PDB ID: 4UD1)[27] and MERS-CoV NTD:P3 (solved in this study) and the CTD domain of MERS-CoV N protein (PDB ID: 6G13)[23] were used as rigid bodies in EOM analysis. With the EOM analysis, 1000 models were generated in the beginning as a structural pool. Selected from the SAXS profiles of the structural pool was an ensemble of models that could fit the experimental scattering curve with their linear combination. Tetrameric MERS-CoV NP conformations and 16-mer MERS-CoV:P3 conformations were selected because their ensemble generated curves fit best to the experimental SAXS results.

Viral Infection. Vero E6 cells (ATCC No: CRL-1586) were seeded onto culture plates with complete Dulbecco's modified Eagle's medium (DMEM) and incubated overnight prior to infection. MERS-CoV (HCoV-EMC/2012) at a multiplicity of infection (M.O.I.) of 0.1 was added to the cells and incubated at 37 °C for 1 h, followed by washing thrice with phosphate-buffered saline (PBS) to remove the unattached virus. Fresh complete culture medium was then added to the plates.

Plaque Assay. Vero E6 cells were seeded in 12-well plates and incubated overnight before the assays. Samples containing MERS-CoV were serially diluted 10× with MEM, added to the wells, and incubated for 1 h with agitation every 15 min. After incubation, the inocula were removed and washed with PBS. An overlay medium comprising 2× MEM and 1.5% (w/v) agarose (1:1) was added to the wells followed by incubation at 37 °C and 5% CO_2 for 3 days. The plates were fixed with 10% (v/v) formalin containing 0.2% (w/v) crystal violet, and the plaques were counted.

RT-qPCR. Total RNA of infected Vero E6 cells was extracted with the RNeasy Mini Kit (Qiagen, Hilden, Germany) according to the manufacturer's instructions. Reverse transcription and PCR amplification were performed with an iTaq Universal One-Step RT-qPCR Kit (Bio-Rad Laboratories, Hercules, CA). Real-time PCR was performed in a StepOnePlus Real-Time PCR System (Applied Biosystems, Foster City, CA). The primer pairs used to amplify the viral RNA were as follows: GAPDH-F: 5′-GAAGGTGAAGGTCG-GAGTC-3′; GAPDH-R: 5′-GAAGATGGTGATGGGATTTC-3′;[52] MERS-CoV-F: 5′-CCACTACTCCCATTTCGTCAG-3′; MERS-CoV-R: 5′-CAGTATGTGTAGTGCGCATATAAGCA-3′.[53] The MERS RNA levels were normalized to that of GAPDH and compared between MERS-CoV groups at 24 h.p.i. and at 48 h.p.i.

Immunofluorescence Assay. Vero E6 cells were seeded in eight-well chamber slides and incubated overnight prior to infection with MERS-CoV at M.O.I. = 0.1. The cells were fixed with 4% (v/v) paraformaldehyde for 20 min at 4 °C, followed by permeabilization in 0.1% (v/v) Triton X-100 for 10 min. Then, 7.5% (v/v) BSA was used as a blocking buffer for 30 min at 37 °C. Anti-MERS-CoV N primary antibody (1:500 dilution; Sino Biological Inc., Beijing, China) was used to stain the virus. The cells were incubated overnight, washed thrice with PBS, and incubated with Alex Fluor 568 anti-rabbit secondary antibody (1:1000 dilution; Thermo Fisher Scientific, Waltham, MA) for 1 h at room temperature. 4′,6-Diamidino-2-phenylindole (DAPI) was added during the PBS wash. MERS nucleocapsid expression was examined under a confocal microscope (LSM-700; Carl Zeiss AG, Oberkochen, Germany).

■ ASSOCIATED CONTENT

Supporting Information

The Supporting Information is available free of charge at https://pubs.acs.org/doi/10.1021/acs.jmedchem.9b01913.

Dimeric conformation of MERS-CoV N-NTD (Figure S1); LibDock pose of dimeric MERS-CoV N-NTD with potent compounds (Figure S2); P3-induced aggregation of the MERS-CoV N protein sequesters the RNA-binding region on the N-CTD dimer (Figure S3); potential target sites for broad-spectrum antiviral compound development (Figure S4); antiviral activity of P3 against MHV (mouse hepatitis virus) (Figure S5); crystallographic data collection and refinement statistics (Table S1); pW43 docking pose with chemical structures, docking scores, and biochemical properties of 17 potential hits (Table S2); primers used for mutagenesis in this study (Table S3); molecular formula strings (PDF)

Molecular Formula Strings_JMC_revision (CSV)

Accession Codes

For PDB codes 6KL2 (native), 6KL5 (N-P1 complex), and 6KL6 (N-P3 complex), authors will release the atomic coordinates and experimental data upon article publication.

■ AUTHOR INFORMATION

Corresponding Author

Ming-Hon Hou − *Institute of Genomics and Bioinformatics and Department of Life Sciences, National Chung Hsing University, Taichung 402, Taiwan;* orcid.org/0000-0003-4170-1527; Phone: +886-4-2284-0338; Email: mhho@nchu.edu.tw; Fax: +886-4-2285-9329

Authors

Shan-Meng Lin − *Institute of Genomics and Bioinformatics and Department of Life Sciences, National Chung Hsing University, Taichung 402, Taiwan*

Shih-Chao Lin − *National Center for Biodefense and Infectious Diseases, School of Systems Biology, George Mason University, Manassas, Virginia 20110, United States;* orcid.org/0000-0003-2942-5937

Jia-Ning Hsu − *Institute of Genomics and Bioinformatics and Department of Life Sciences, National Chung Hsing University, Taichung 402, Taiwan*

Chung-ke Chang − *Institute of Biomedical Sciences, Academia Sinica, Taipei 115, Taiwan*

Ching-Ming Chien − *Institute of Genomics and Bioinformatics and Department of Life Sciences, National Chung Hsing University, Taichung 402, Taiwan*

Yong-Sheng Wang − *Institute of Genomics and Bioinformatics, National Chung Hsing University, Taichung 402, Taiwan*

Hung-Yi Wu − *Graduate Institute of Veterinary Pathobiology, College of Veterinary Medicine, National Chung Hsing University, Taichung 40227, Taiwan*

U-Ser Jeng − *National Synchrotron Radiation Research Center, Hsinchu 30076, Taiwan; Department of Chemical Engineering, National Tsing Hua University, Hsinchu 30013, Taiwan;* orcid.org/0000-0002-2247-5061

Kylene Kehn-Hall − *National Center for Biodefense and Infectious Diseases, School of Systems Biology, George Mason University, Manassas, Virginia 20110, United States*

Complete contact information is available at: https://pubs.acs.org/10.1021/acs.jmedchem.9b01913

Author Contributions

○S.-M.L., S.-C.L., J.-N.H., and C.-k.C. contributed equally to this work.

Author Contributions

Jia N. Hsu, Shih C. Lin, Yong S. Wang, and Ming H. Hou designed research; Jia N. Hsu, Shih C. Lin, Shan M. Lin, Ching M. Chien, and Yong S. Wang performed research; Hung Y. Wu, U S. Jeng, K. Kehn-Hall, and Ming H. Hou contributed new reagents or analytic tools; Shih C. Lin, Shan M. Lin, Ching M. Chien, and Ming H. Hou analyzed the data; Shih C. Lin, Shan M. Lin, Chung K. Chang, Ching M. Chien, and Ming H. Hou wrote the paper.

https://dx.doi.org/10.1021/acs.jmedchem.9b01913
J. Med. Chem. 2020, 63, 3131−3141

Funding

This work was supported by the MOST 106-2628-M-005-001-MY3.

Notes

The authors declare no competing financial interest.

■ ACKNOWLEDGMENTS

We thank the National Synchrotron Radiation Research Center (Taiwan) and the synchrotron radiation facility SPring-8 (Japan) for X-ray diffraction data collection.

■ ABBREVIATIONS

PPIs, protein−protein interactions; MERS-CoV, Middle East Respiratory Syndrome Coronavirus; NTD, N-terminal domain; CTD, C-terminal domain; N, nucleocapsid; β-CoVs, betacoronavirus; RNP, ribonucleoprotein; SAXS, small-angle X-ray scattering; MR, molecular replacement; BSA, buried surface areas; TPSA, topological polar surface areas; CC_{50}, cytotoxic concentration; EC_{50}, effective concentration; D_{max}, maximum dimension; R_g, radius of gyration; MHV, mouse hepatitis virus

■ REFERENCES

(1) Bosch, J. PPI inhibitor and stabilizer development in human diseases. *Drug Discovery Today: Technol.* **2017**, *24*, 3−9.
(2) Sijbesma, E.; Hallenbeck, K. K.; Leysen, S.; de Vink, P. J.; Skóra, L.; Jahnke, W.; Brunsveld, L.; Arkin, M. R.; Ottmann, C. Site-directed fragment-based screening for the discovery of protein−protein interaction stabilizers. *J. Am. Chem. Soc.* **2019**, *141*, 3524−3531.
(3) Stevers, L. M.; Sijbesma, E.; Botta, M.; MacKintosh, C.; Obsil, T.; Landrieu, I.; Cau, Y.; Wilson, A. J.; Karawajczyk, A.; Eickhoff, J.; Davis, J.; Hann, M.; O'Mahony, G.; Doveston, R. G.; Brunsveld, L.; Ottmann, C. Modulators of 14-3-3 protein-protein interactions. *J. Med. Chem.* **2018**, *61*, 3755−3778.
(4) Ni, D.; Lu, S.; Zhang, J. Emerging roles of allosteric modulators in the regulation of protein-protein interactions (PPIs): a new paradigm for PPI drug discovery. *Med. Res. Rev.* **2019**, *39*, 2314−2342.
(5) Fischer, G.; Rossmann, M.; Hyvonen, M. Alternative modulation of protein-protein interactions by small molecules. *Curr. Opin. Biotechnol.* **2015**, *35*, 78−85.
(6) Petta, I.; Lievens, S.; Libert, C.; Tavernier, J.; De Bosscher, K. Modulation of protein-protein interactions for the development of novel therapeutics. *Mol. Ther.* **2016**, *24*, 707−718.
(7) Zhong, M.; Lee, G. M.; Sijbesma, E.; Ottmann, C.; Arkin, M. R. Modulating protein-protein interaction networks in protein homeostasis. *Curr. Opin. Chem. Biol.* **2019**, *50*, 55−65.
(8) Yang, C. H.; Horwitz, S. B. Taxol: the first microtubule stabilizing agent. *Int. J. Mol. Sci.* **2017**, *18*, No. 1733.
(9) Yuan, Y.; Wang, L.; Du, W.; Ding, Z.; Zhang, J.; Han, T.; An, L.; Zhang, H.; Liang, G. Intracellular self-assembly of taxol nanoparticles for overcoming multidrug resistance. *Angew. Chem., Int. Ed.* **2015**, *54*, 9700−9704.
(10) Saxton, R. A.; Sabatini, D. M. mTOR signaling in gowth, metabolism, and disease. *Cell* **2017**, *168*, 960−976.
(11) White, K. M.; Abreu, P.; Wang, H.; De Jesus, P. D.; Manicassamy, B.; García-Sastre, A.; Chanda, S. K.; DeVita, R. J.; Shaw, M. L. Broad spectrum inhibitor of influenza A and B viruses targeting the viral nucleoprotein. *ACS Infect. Dis.* **2018**, *4*, 146−157.
(12) Zaki, A. M.; van Boheemen, S.; Bestebroer, T. M.; Osterhaus, A. D.; Fouchier, R. A. Isolation of a novel coronavirus from a man with pneumonia in saudi arabia. *N. Engl. J. Med.* **2012**, *367*, 1814−1820.
(13) Forni, D.; Cagliani, R.; Clerici, M.; Sironi, M. Molecular evolution of human coronavirus genomes. *Trends Microbiol.* **2017**, *25*, 35−48.
(14) Mubarak, A.; Alturaiki, W.; Hemida, M. G. Middle east respiratory syndrome coronavirus (MERS-CoV): infection, immunological response, and vaccine development. *J. Immunol. Res.* **2019**, *2019*, 1−11.
(15) Zhu, N.; Zhang, D.; Wang, W.; Li, X.; Yang, B.; Song, J.; Zhao, X.; Huang, B.; Shi, W.; Lu, R.; Niu, P.; Zhan, F.; Ma, X.; Wang, D.; Xu, W.; Wu, G.; Gao, G. F.; Tan, W. A novel coronavirus from patients with pneumonia in china, 2019. *N. Engl. J. Med.* **2020**, 1−7.
(16) Hui, D. S.; E, I. A.; Madani, T. A.; Ntoumi, F.; Kock, R.; Dar, O.; Ippolito, G.; McHugh, T. D.; Memish, Z. A.; Drosten, C.; Zumla, A.; Petersen, E. The continuing 2019-nCoV epidemic threat of novel coronaviruses to global health - the latest 2019 novel coronavirus outbreak in wuhan, china. *Int. J. Infect. Dis.* **2020**, *91*, 264−266.
(17) Huang, X.; Li, M.; Xu, Y.; Zhang, J.; Meng, X.; An, X.; Sun, L.; Guo, L.; Shan, X.; Ge, J.; Chen, J.; Luo, Y.; Wu, H.; Zhang, Y.; Jiang, Q.; Ning, X. Novel gold nanorod-based HR1 peptide inhibitor for middle east respiratory syndrome coronavirus. *ACS Appl. Mater. Interfaces* **2019**, *11*, 19799−19807.
(18) Chang, C. K.; Lo, S. C.; Wang, Y. S.; Hou, M. H. Recent insights into the development of therapeutics against coronavirus diseases by targeting N protein. *Drug Discovery Today* **2016**, *21*, 562−572.
(19) Zumla, A.; Chan, J. F.; Azhar, E. I.; Hui, D. S.; Yuen, K. Y. Coronaviruses - drug discovery and therapeutic options. *Nat. Rev. Drug Discovery* **2016**, *15*, 327−347.
(20) McBride, R.; van Zyl, M.; Fielding, B. C. The coronavirus nucleocapsid is a multifunctional protein. *Viruses* **2014**, *6*, 2991−3018.
(21) de Wit, E.; van Doremalen, N.; Falzarano, D.; Munster, V. J. SARS and MERS: recent insights into emerging coronaviruses. *Nat. Rev. Microbiol.* **2016**, *14*, 523−534.
(22) Lin, S. Y.; Liu, C. L.; Chang, Y. M.; Zhao, J.; Perlman, S.; Hou, M. H. Structural basis for the identification of the N-terminal domain of coronavirus nucleocapsid protein as an antiviral target. *J. Med. Chem.* **2014**, *57*, 2247−2257.
(23) Nguyen, T. H. V.; Lichiere, J.; Canard, B.; Papageorgiou, N.; Attoumani, S.; Ferron, F.; Coutard, B. Structure and oligomerization state of the C-terminal region of the middle east respiratory syndrome coronavirus nucleoprotein. *Acta Crystallogr., Sect. D: Struct. Biol.* **2019**, *75*, 8−15.
(24) Chen, I. J.; Yuann, J. M.; Chang, Y. M.; Lin, S. Y.; Zhao, J.; Perlman, S.; Shen, Y. Y.; Huang, T. H.; Hou, M. H. Crystal structure-based exploration of the important role of Arg106 in the RNA-binding domain of human coronavirus OC43 nucleocapsid protein. *Biochim. Biophys. Acta, Proteins Proteomics* **2013**, *1834*, 1054−1062.
(25) Fan, H.; Ooi, A.; Tan, Y. W.; Wang, S.; Fang, S.; Liu, D. X.; Lescar, J. The nucleocapsid protein of coronavirus infectious bronchitis virus: crystal structure of its N-terminal domain and multimerization properties. *Structure* **2005**, *13*, 1859−1868.
(26) Chen, J.; Sawyer, N.; Regan, L. Protein-protein interactions: general trends in the relationship between binding affinity and interfacial buried surface area. *Protein Sci.* **2013**, *22*, 510−515.
(27) Papageorgiou, N.; Lichiere, J.; Baklouti, A.; Ferron, F.; Sevajol, M.; Canard, B.; Coutard, B. Structural characterization of the N-terminal part of the MERS-CoV nucleocapsid by X-ray diffraction and small-angle X-ray scattering. *Acta Crystallogr., Sect. D: Struct. Biol.* **2016**, *72*, 192−202.
(28) Jayaram, H.; Fan, H.; Bowman, B. R.; Ooi, A.; Jayaram, J.; Collisson, E. W.; Lescar, J.; Prasad, B. V. X-ray structures of the N- and C-terminal domains of a coronavirus nucleocapsid protein: implications for nucleocapsid formation. *J. Virol.* **2006**, *80*, 6612−6620.
(29) Saikatendu, K. S.; Joseph, J. S.; Subramanian, V.; Neuman, B. W.; Buchmeier, M. J.; Stevens, R. C.; Kuhn, P. Ribonucleocapsid formation of severe acute respiratory syndrome coronavirus through molecular action of the N-terminal domain of N protein. *J. Virol.* **2007**, *81*, 3913−3921.
(30) Grossoehme, N. E.; Li, L.; Keane, S. C.; Liu, P.; Dann, C. E., 3rd; Leibowitz, J. L.; Giedroc, D. P. Coronavirus N protein N-

terminal domain (NTD) specifically binds the transcriptional regulatory sequence (TRS) and melts TRS-cTRS RNA duplexes. *J. Mol. Biol.* **2009**, *394*, 544−557.
(31) Pyrkov, T. V.; Chugunov, A. O.; Krylov, N. A.; Nolde, D. E.; Efremov, R. G. PLATINUM: a web tool for analysis of hydrophobic/hydrophilic organization of biomolecular complexes. *Bioinformatics* **2009**, *25*, 1201−1202.
(32) Broos, J.; Tveen-Jensen, K.; de Waal, E.; Hesp, B. H.; Jackson, J. B.; Canters, G. W.; Callis, P. R. The emitting state of tryptophan in proteins with highly blue-shifted fluorescence. *Angew. Chem., Int. Ed.* **2007**, *46*, 5137−5139.
(33) Gui, M.; Liu, X.; Guo, D.; Zhang, Z.; Yin, C.-C.; Chen, Y.; Xiang, Y. Electron microscopy studies of the coronavirus ribonucleoprotein complex. *Protein Cell* **2017**, *8*, 219−224.
(34) Chen, C. Y.; Chang, C. K.; Chang, Y. W.; Sue, S. C.; Bai, H. I.; Riang, L.; Hsiao, C. D.; Huang, T. H. Structure of the SARS coronavirus nucleocapsid protein RNA-binding dimerization domain suggests a mechanism for helical packaging of viral RNA. *J. Mol. Biol.* **2007**, *368*, 1075−1086.
(35) Wichapong, K.; Poelman, H.; Ercig, B.; Hrdinova, J.; Liu, X.; Lutgens, E.; Nicolaes, G. A. Rational modulator design by exploitation of protein-protein complex structures. *Future Med. Chem.* **2019**, *11*, 1015−1033.
(36) de Vink, P. J.; Andrei, S. A.; Higuchi, Y.; Ottmann, C.; Milroy, L. G.; Brunsveld, L. Cooperativity basis for small-molecule stabilization of protein-protein interactions. *Chem. Sci.* **2019**, *10*, 2869−2874.
(37) Blevitt, J. M.; Hack, M. D.; Herman, K. L.; Jackson, P. F.; Krawczuk, P. J.; Lebsack, A. D.; Liu, A. X.; Mirzadegan, T.; Nelen, M. I.; Patrick, A. N.; Steinbacher, S.; Milla, M. E.; Lumb, K. J. Structural basis of small-molecule aggregate induced inhibition of a protein-protein interaction. *J. Med. Chem.* **2017**, *60*, 3511−3517.
(38) Spencer-Smith, R.; Koide, A.; Zhou, Y.; Eguchi, R. R.; Sha, F.; Gajwani, P.; Santana, D.; Gupta, A.; Jacobs, M.; Herrero-Garcia, E.; Cobbert, J.; Lavoie, H.; Smith, M.; Rajakulendran, T.; Dowdell, E.; Okur, M. N.; Dementieva, I.; Sicheri, F.; Therrien, M.; Hancock, J. F.; Ikura, M.; Koide, S.; O'Bryan, J. P. Inhibition of RAS function through targeting an allosteric regulatory site. *Nat. Chem. Biol.* **2017**, *13*, 62−68.
(39) Pang, B.; Cheung, N. N.; Zhang, W.; Dai, J.; Kao, R. Y.; Zhang, H.; Hao, Q. Structural characterization of H1N1 nucleoprotein-nucleozin binding sites. *Sci. Rep.* **2016**, *6*, No. 195.
(40) Kao, R. Y.; Yang, D.; Lau, L. S.; Tsui, W. H.; Hu, L.; Dai, J.; Chan, M. P.; Chan, C. M.; Wang, P.; Zheng, B. J.; Sun, J.; Huang, J. D.; Madar, J.; Chen, G.; Chen, H.; Guan, Y.; Yuen, K. Y. Identification of influenza A nucleoprotein as an antiviral target. *Nat. Biotechnol.* **2010**, *28*, 600−605.
(41) Klenchin, V. A.; King, R.; Tanaka, J.; Marriott, G.; Rayment, I. Structural basis of swinholide A binding to actin. *Chem. Biol.* **2005**, *12*, 287−291.
(42) Shin, I.; Hong, S.; Krische, M. J. Total synthesis of swinholide A: an exposition in hydrogen-mediated C−C bond formation. *J. Am. Chem. Soc.* **2016**, *138*, 14246−14249.
(43) Bubb, M. R.; Spector, I.; Bershadsky, A. D.; Korn, E. D. Swinholide A is a microfilament disrupting marine toxin that stabilizes actin dimers and severs actin filaments. *J. Biol. Chem.* **1995**, *270*, 3463−3466.
(44) Ferreira de Freitas, R.; Schapira, M. A systematic analysis of atomic protein-ligand interactions in the PDB. *MedChemComm* **2017**, *8*, 1970−1981.
(45) Hossain, B. M.; Konermann, L. Pulsed hydrogen/deuterium exchange MS/MS for studying the relationship between noncovalent protein complexes in solution and in the gas phase after electrospray ionization. *Anal. Chem.* **2006**, *78*, 1613−1619.
(46) Wang, Y. S.; Chang, C. K.; Hou, M. H. Crystallographic analysis of the N-terminal domain of middle east respiratory syndrome coronavirus nucleocapsid protein. *Acta Crystallogr., Sect. F: Struct. Biol. Commun.* **2015**, *71*, 977−980.
(47) Adams, P.; Grosse-Kunstleve, R. W.; Hung, L.-W.; Ioerger, T. R.; McCoy, A. J.; Moriarty, N.; Read, R. J.; Sacchettini, J. C.; Sauter, N.; Terwilliger, T. PHENIX: building new software for automated crystallographic structure determination. *Acta Crystallogr., Sect. D: Biol. Crystallogr.* **2002**, *58*, 1948−1954.
(48) Emsley, P.; Cowtan, K. Coot: model-building tools for molecular graphics. *Acta Crystallogr., Sect. D: Biol. Crystallogr.* **2004**, *60*, 2126−2132.
(49) *The PyMOL Molecular Graphics System*, version 1.8; Schrodinger, LLC, 2015.
(50) Petoukhov, M. V.; Franke, D.; Shkumatov, A. V.; Tria, G.; Kikhney, A. G.; Gajda, M.; Gorba, C.; Mertens, H. D.; Konarev, P. V.; Svergun, D. I. New developments in the ATSAS program package for small-angle scattering data analysis. *J. Appl. Crystallogr.* **2012**, *45*, 342−350.
(51) Svergun, D.; Barberato, C.; Koch, M. H. J. CRYSOL - a program to evaluate X-ray solution scattering of biological macromolecules from atomic coordinates. *J. Appl. Crystallogr.* **1995**, *28*, 768−773.
(52) Gunalan, V.; Mirazimi, A.; Tan, Y. J. A putative diacidic motif in the SARS-CoV ORF6 protein influences its subcellular localization and suppression of expression of co-transfected expression constructs. *BMC Res Notes* **2011**, *4*, No. 446.
(53) Furuse, Y.; Okamoto, M.; Oshitani, H. Conservation of nucleotide sequences for molecular diagnosis of middle east respiratory syndrome coronavirus, 2015. *Int. J. Infect. Dis.* **2015**, *40*, 25−27.

https://dx.doi.org/10.1021/acs.jmedchem.9b01913
J. Med. Chem. 2020, 63, 3131−3141